PORFLOW Modeling Supporting the FY14 Saltstone Special Analysis

G. P. Flach
G. A. Taylor

April 2014

SRNL-STI-2014-00083, Revision 1

DISCLAIMER

Printed in the United States of America

Prepared for
U.S. Department of Energy

SRNL-STI-2014-00083
Revision 1

Keywords: *Saltstone, Special Analysis*

Retention: *Permanent*

PORFLOW Modeling Supporting the FY14 Saltstone Special Analysis

G. P. Flach
G. A. Taylor

April 2014

Prepared for the U.S. Department of Energy under contract number DE-AC09-08SR22470.

Savannah River National Laboratory™
OPERATED BY SAVANNAH RIVER NUCLEAR SOLUTIONS

REVIEWS AND APPROVALS

AUTHORS:

G. P. Flach, Radiological Performance Assessment — Date: 4/1/2014

G. A. Taylor, Radiological Performance Assessment — Date: 4/1/2014

TECHNICAL REVIEW:

F. G. Smith, Process Modeling & Computational Chemistry, Reviewed per E7 2.60 — Date: 4/1/2014

APPROVAL:

D. A. Crowley, Manager
Radiological Performance Assessment — Date: 4/1/14

R. S. Aylward, Manager
Environmental Restoration Technologies — Date: 4/1/14

K. H. Rosenberger, Manager
Waste Disposal Authority — Date: 4/1/2014

REVISIONS

Revision	Description
0	Original issue
1	Corrections to transcription errors in Table 2-1. Annotation added to Figure 4-1 for clarification.

EXECUTIVE SUMMARY

PORFLOW related analyses supporting the Saltstone FY14 Special Analysis (SA) described herein are based on prior modeling supporting the Saltstone FY13 SA. Notable changes to the previous round of simulations include: a) consideration of Saltstone Disposal Unit (SDU) design type 6 under "Nominal" and "Margin" conditions, b) omission of the clean cap fill from the nominal SDU 2 and 6 modeling cases as a reasonable approximation of greater waste grout fill heights, c) minor updates to the cementitious materials degradation analysis, d) use of updated I-129 sorption coefficient (K_d) values in soils, e) assignment of the pH/Eh environment of saltstone to the underlying floor concrete, considering down flow through an SDU, and f) implementation of an improved sub-model for Tc release in an oxidizing environment. These new model developments are discussed and followed by a cursory presentation of simulation results. The new Tc release sub-model produced significantly improved (smoother) flux results compared to the FY13 SA. Further discussion of PORFLOW model setup and simulation results will be presented in the FY14 SA, including dose results.

TABLE OF CONTENTS

LIST OF TABLES

LIST OF FIGURES

LIST OF ABBREVIATIONS

BE	Best Estimate
DFM	Discrete Fracture Model
FY	Fiscal Year
NV	Nominal Value
SA	Special Analysis
SDU	Saltstone Disposal Unit
SRNL	Savannah River National Laboratory
SRR	Savannah River Remediation

1.0 Introduction

PORFLOW related analyses supporting the Saltstone FY14 Special Analysis (SA) (SRR 2014) described herein are based on PORFLOW modeling (Jordan and Flach 2013) supporting the Saltstone FY13 SA (SRR 2013). Modeling scenarios, key inputs, and work scope are specified in the Task Technical Request (Sheppard 2013) and Task Technical & Quality Assurance Plan (Taylor 2013). Notable changes to the previous round of simulations include: a) consideration of Saltstone Disposal Unit (SDU) design type 6 under "Nominal" and "Margin" conditions, b) omission of the clean cap fill from the nominal SDU 2 and 6 modeling cases as a reasonable approximation of greater waste grout fill heights (Flach 2013), c) minor updates to the cementitious materials degradation analysis (Flach and Smith 2013), d) use of updated I-129 sorption coefficient (K_d) values in soils, e) assignment of the pH/Eh environment of saltstone to the underlying floor concrete, considering down flow through an SDU, and f) implementation of an improved sub-model for Tc release in an oxidizing environment. These new model developments are discussed in the next section, followed by a cursory presentation of simulation results. Further discussion of PORFLOW model setup and simulation results is presented in the FY14 SA (SRR 2014), including dose results.

2.0 General Model Revisions

The material zones represented on the PORFLOW numerical grids for SDU design types 1, 2, 4, and 6 are illustrated in Figure 2-1 through Figure 2-4, respectively. SDU 2 and 6 include a column feature that aggregates multiple physical columns into a single grid column; the column region is further subdivided into vertical segments that are approximately two feet in length. Although separate SALTSTONE and CLEAN_GROUT material zones are retained in the FY14 SA for SDU 2 and 6, the same "`saltstone`" material is assigned to both grid regions, and the waste inventory is spread uniformly through both zones.

The revised cementitious material degradation analysis produced minor differences in degradation times, except for SDU 2 and 6 roof concrete. The current modeling scenario for these units omits the clean cap fill between waste grout and the roof (Flach 2013). Previously, external sulfate attack on the underside of the roof was delayed because of the sulfate-free clean cap. Without the clean cap, the roof is exposed immediately to sulfate attack resulting in earlier degradation times. Table 2-1 summarizes degradations time from Flach and Smith (2013), and Table 2-2 through Table 2-4 present degradation times for specific grout segments. Table 2-2 also presents the fictitious negative starting times for SDU 6 wall degradation that are used to implement initial (t=0) wall degradation from exposure to wet grout and/or bleedwater during facility operation. SDU 2 incorporates an interior waterproof coating and the full wall thickness is considered undegraded at time zero.

Transport parameters for cementitious materials are generally based on the pH and Eh state of the material, which is defined through discrete transitions defined in terms of pore volumes. Following flow simulation, the velocity field and the two pore volume transitions (moderate age → old age, reduced → oxidized) are used to calculate the time of the pH and Eh transitions. The FY14 SA incorporates a refinement to pore volume counting for the concrete floor. By default, soil moisture or groundwater is assumed to be the fluid infiltrating a material zone. For the FLOOR grid zone, the infiltrating fluid is primarily high pH, reducing leachate from the overlying SALTSTONE grid zone, because flow is predominantly downward through the facility and species transport is advection dominated. Therefore, the floor is not exposed to infiltrating oxygen or low pH water until after the Eh and pH transitions, respectively, occur in the saltstone. For simplicity and as a conservatism, the lag times between the saltstone and floor pH and Eh transitions are ignored. Rather, the floor concrete is assumed to experience pH/Eh transitions at the same times as saltstone.

Discrete pH/Eh transitions based on pore volume counting are applied to all nuclides except Tc-99. Transport of Tc-99 is based on a more sophisticated shrinking core model of slag oxidation, and includes solubility controlled Tc release under reducing conditions (Jordan and Flach 2013). The Tc transport sub-model was revised for the FY14 SA to reduce artificial numerical spikes related to how Tc transitions from a reduced (IV) to oxidized (VII) state while the slag in a grid cell is being oxidized. The revised Tc release sub-model is presented in the next section.

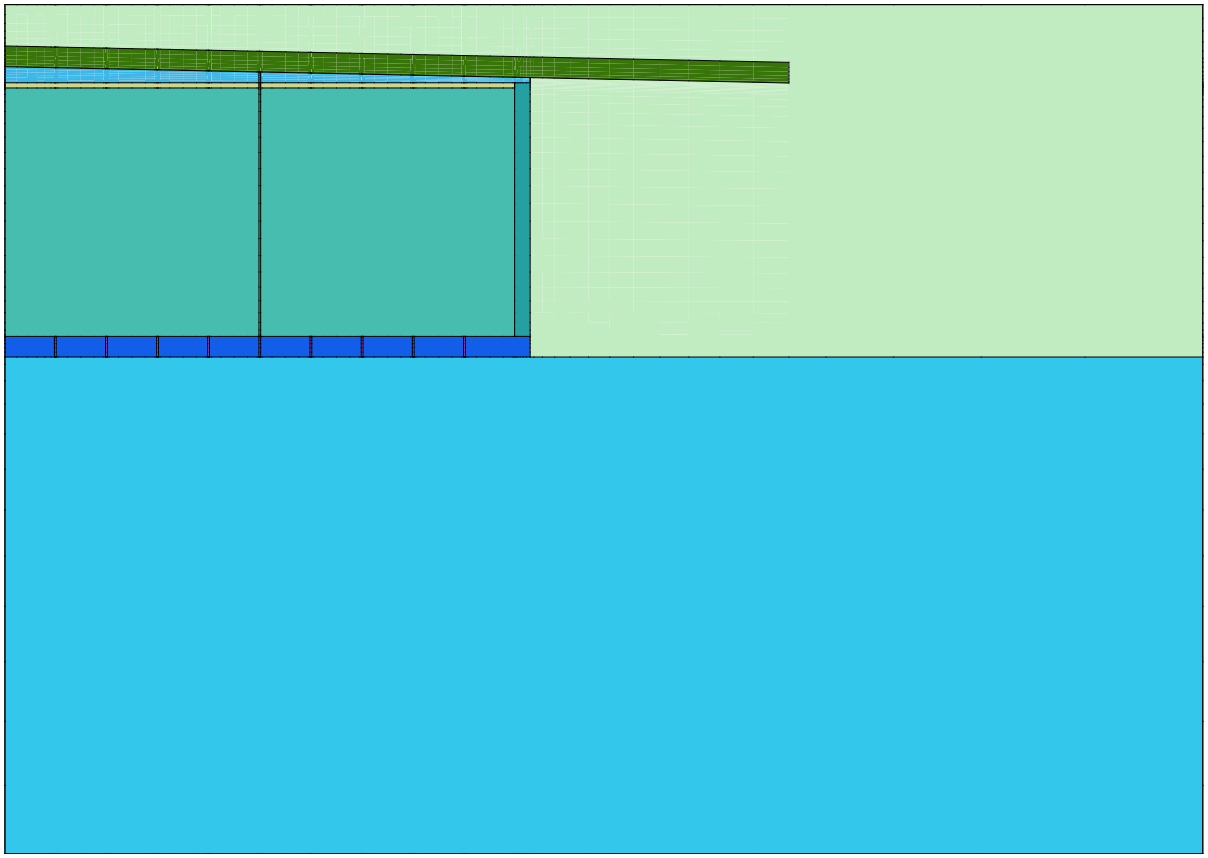

Figure 2-1. Material zones in SDU 1 computational grid.

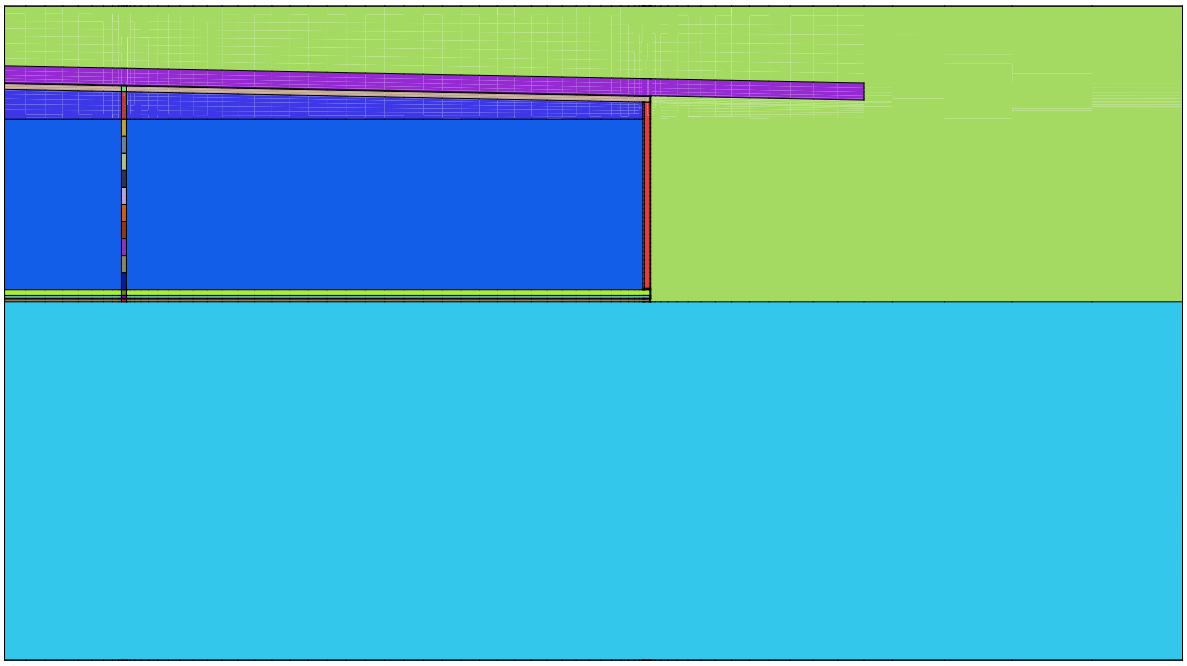

Figure 2-2. Material zones in SDU 2 computational grid.

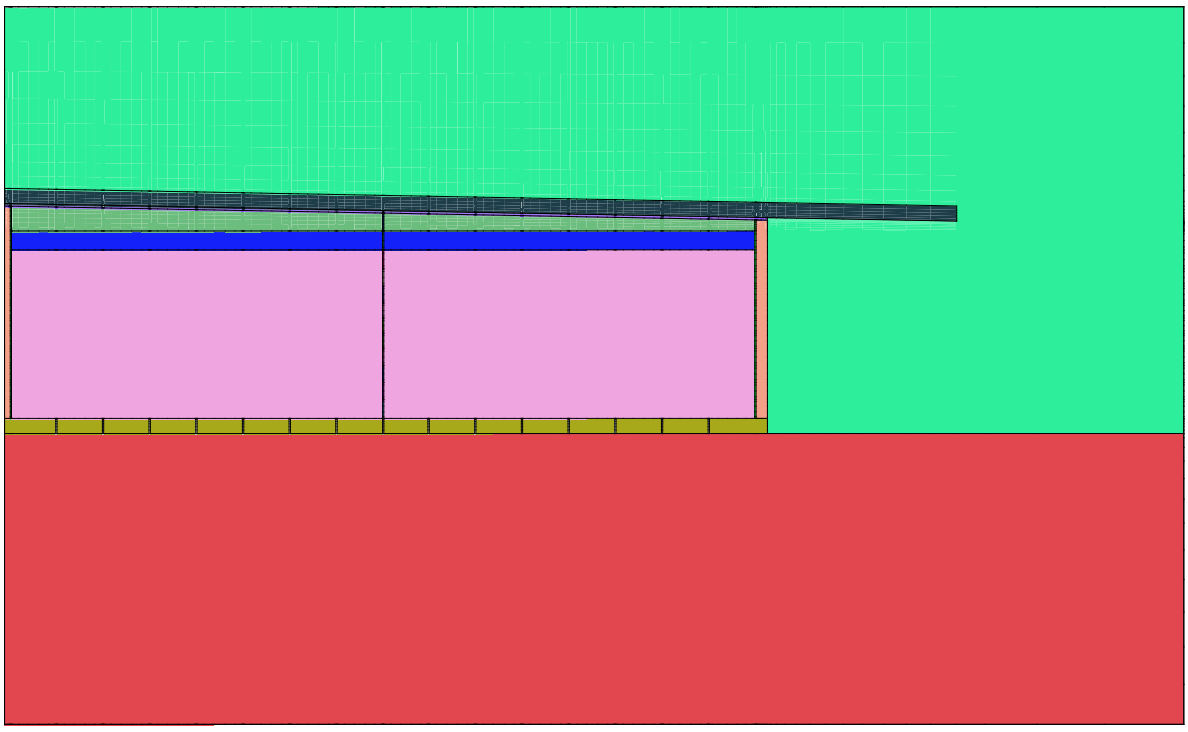

Figure 2-3. Material zones in SDU 4 computational grid.

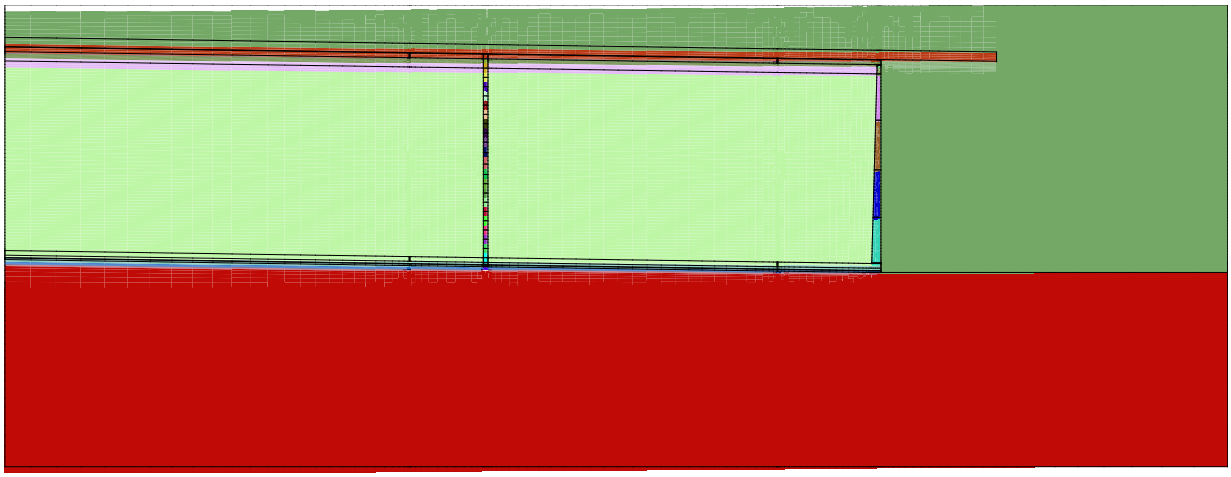

Figure 2-4. Material zones in SDU 6 computational grid.

Table 2-1. Cementitious material degradation times (Flach and Smith 2013).

	SDU6				SDU2				SDU4				SDU1			
	Thickness:		NV	BE	Thickness:		NV	BE	Thickness:		NV	BE	Thickness:		NV	BE
Component	(in)	(cm)	(yr)	(yr)	(in)	(cm)	(yr)	(yr)	(in)	(cm)	(yr)	(yr)	(in)	(cm)	(yr)	(yr)
Roof delay			**0**	**0**			**0**	**0**			**0**	**0**			**0**	**0**
Roof delay+degradation	12	30.48	**1413**	**2717**	8	20	**961**	**1820**	4	10	**1106**	**7237**	6	15	**486**	**1687**
FloorUMM delay			**0**	**0**			**0**	**0**			**0**	**0**			**0**	**0**
FloorUMM delay+degradation	12	30.48	**1413**	**2717**	12	30	**1413**	**2717**	24	61	**1404**	**3868**	24	61	**1404**	**3868**
Wall 5 delay			**0**	**0**			**0**	**0**								
Wall delay+degradation	8.75	22.23	**817**	**1937**	8	20	**922**	**1797**								
Wall 4 delay			**0**	**0**												
Wall 2 delay+degradation	10.47	26.59	**981**	**2329**												
Wall 3 delay			**0**	**0**												
Wall 3 delay+degradation	13.5	34.29	**1265**	**3021**												
Wall 2 delay			**0**	**0**												
Wall 4 delay+degradation	16.55	42.04	**1550**	**3720**												
Wall 1 delay			**0**	**0**												
Wall 5 delay+degradation	19.5	49.53	**1827**	**4397**												
Grout - 3.45' delay											**2113**	**57714**				
Grout - 3.45' delay+degradation									273	693	**233838**	**2374962**				
Grout delay			**1413**	**2717**			**961**	**1820**			**1106**	**7237**			**486**	**1687**
Grout delay+degradation	516	1311	**439398**	**4382571**	264	671	**225047**	**2242676**	41	105	**2113**	**57714**	294	747	**250036**	**2497186**
Column delay			**1413**	**2717**			**961**	**1820**			**1106**	**3868**				
Column delay+degradation	24	60.96	**1996**	**32000**	24	61	**1545**	**31103**	24	61	**1690**	**33151**				

Table 2-2. Wall (left) and grout (right) segment degradation times for SDU 6 under Nominal Value (NV) and Best Estimate (BE) conditions.

SDU 6

NV

	Initial thickness (in)	Initial thickness (cm)	t=0 thickness (in)	t=0 thickness (cm)	Times: (yr)
⑤	10.35	26.3	8.75	22.2	**-149** 817 **817**
④	12.28	31.2	10.47	26.6	**-170** 981 **981**
③	15.66	39.8	13.5	34.3	**-202** 1265 **1265**
②	19.07	48.4	16.55	42.0	**-236** 1550 **1550**
①	22.37	56.8	19.5	49.5	**-269** 1827 **1827**

NV

segment	start (yr)	end (yr)	segment
grout1	1413	1997	grout21
grout2	1997	2581	grout20
grout3	2581	3165	grout19
grout4	3165	3749	grout18
grout5	3749	4333	grout17
grout6	4333	4917	grout16
grout7	4917	5501	grout15
grout8	5501	6085	grout14
grout9	6085	6669	grout13
grout10	6669	7253	grout12
grout11	7253	7837	grout11

BE

	Initial thickness (in)	Initial thickness (cm)	t=0 thickness (in)	t=0 thickness (cm)	Times: (yr)
⑤	10.35	26.3	8.75	22.2	**-354** 1937 **1937**
④	12.28	31.2	10.47	26.6	**-403** 2329 **2329**
③	15.66	39.8	13.5	34.3	**-483** 3021 **3021**
②	19.07	48.4	16.55	42.0	**-566** 3720 **3720**
①	22.37	56.8	19.5	49.5	**-647** 4397 **4397**

BE

segment	start (yr)	end (yr)	segment
grout1	2717	32000	grout21
grout2	32000	61283	grout20
grout3	61283	90566	grout19
grout4	90566	119849	grout18
grout5	119849	149132	grout17
grout6	149132	178415	grout16
grout7	178415	207698	grout15
grout8	207698	236981	grout14
grout9	236981	266264	grout13
grout10	266264	295547	grout12
grout11	295547	324830	grout11

Table 2-3. Grout segment degradation times for SDU 2.

SDU 2			
NV			
segment	start (yr)	end (yr)	segment
grout1	961	1545	grout11
grout2	1545	2129	grout10
grout3	2129	2713	grout9
grout4	2713	3297	grout8
grout5	3297	3881	grout7
grout6	3881	4465	grout6
BE			
segment	start (yr)	end (yr)	segment
grout1	1820	31103	grout11
grout2	31103	60386	grout10
grout3	60386	89669	grout9
grout4	89669	118952	grout8
grout5	118952	148235	grout7
grout6	148235	177518	grout6

Table 2-4. Grout segment degradation times for SDU 4.

SDU 4			
segment	start (yr)	end (yr)	segment
grout1	1106	1690	grout12
grout2	1690	2274	grout11
grout3	2274	2858	grout10
grout4	2858	3442	grout9
grout5	3442	4026	grout8
grout6	4026	4610	grout7

3.0 Tc Release Sub-Model Development

The transport properties of Tc recommended for cementitious materials are listed in Table 3-1. The general sequence for saltstone is Reduced / Young → Reduced / Moderate → Oxidized / Moderate → Oxidized / Aged. The pH transition from Young to Moderate age occurs relatively quickly in the context of PA timeframes and is ignored in PORFLOW modeling, that is, PA simulations start with Reduced and Moderately-aged saltstone. The primary variability in Tc mobility arises from the Eh transition from Reduced to Oxidized conditions at Moderate age. The pH transition from Moderate to Aged, if it occurs with the simulation period, corresponds to a relatively small change in sorption coefficient and is also ignored. Thus PORFLOW simulations consider only an Eh transition from solubility control at 1.0E-8 mol/L to sorption control with K_d = 0.5 mL/g, the latter conservatively chosen as the minimum of the Moderate and Aged values.

Table 3-1. Tc transport parameters recommended for cementitious materials (Kaplan and Li 2013).

Cementitious Material	**Young Cement 1st Stage (pH ~12)**	**Moderately-aged Cement 2nd Stage (pH ~10.5)**	**Aged Cement 3rd Stage (pH ~5.5)**
Reduced	6 x 10^{-7} mol/L solubility	1 x 10^{-8} mol/L solubility	0.5 mL/g sorption (K_d)
Oxidized	0.8 mL/g sorption (K_d)	0.8 mL/g sorption (K_d)	0.5 mL/g sorption (K_d)

The oxidation state of saltstone is simulated in PORFLOW by a shrinking core model of slag oxidation following Kaplan and Hang (2003). A slag reduction (reaction) capacity is defined as a solid-phase concentration expressed in units of milliequivalents per gram (meq/g). Dissolved oxygen at its solubility limit, introduced through boundaries and internal sources, migrates through advection and/or diffusion into saltstone and consumes the slag reaction capacity. The oxidation fraction of each cell, ranging from 0 to 1, is tracked through time for each computational cell.

PORFLOW version 6.30.2 does not provide a built-in means for implementing both solubility control under reducing conditions, and a transition from solubility to sorption control as a function of oxidation fraction. However, both phenomena can be implemented through a user-defined effective sorption coefficient function that varies from cell to cell through time. In the FY13 SA combined solubility and oxidation control was implemented through the effective sorption coefficient function (Jordan and Flach 2013) summarized by

$$K_d = (1 - {x_{Ox}}^p) \cdot max\left[\frac{c_T - nSC_{sol}}{\rho_b C_{sol}}, K_{d,Re}\right] + {x_{Ox}}^p \cdot K_{d,Ox} \quad (1)$$

where K_d = sorption coefficient, x_{Ox} = oxidized fraction of slag, $K_{d,Re}$ = a minimum under reducing conditions, c_T = total bulk Tc concentration (m_{Tc}/V) (i.e., mass of Tc divided by total volume), n = porosity, S = saturation, c_{sol} = Tc solubility limit under reducing conditions, ρ_b = bulk density, $K_{d,Ox}$ = sorption coefficient under oxidized conditions, and p = user-selected exponent = 25 (Jordan and Flach 2013). Going forward this K_d model embedded within the overall Tc transport model will be referred to as the FY13 SA Tc release sub-model.

Figure 3-1(a) and Figure 3-2 illustrate the conceptual basis and qualitative behavior of the FY13 SA Tc release sub-model. The FY13 SA model assumes a well-mixed computational cell, such that most or all of the slag reaction capacity must be depleted before an oxidized condition is achieved and Tc is released to the liquid phase (as solubility control goes away). The concept creates an abrupt drop in sorption

coefficient and spike release of Tc as the oxidation process within an individual cell reaches completion. On a computational grid of multiple cells, this behavior manifests itself as periodic spikes in the Tc flux leaving the modeling domain as particular cells, or small groups of cells, approach 100% oxidation. Examples include Figures 2-30, 4-2 (F-3), 4-11 (F14), and 5-4 through 5-6 in Jordan and Flach (2013). These discrete spikes reflect numerical discretization rather than any real phenomenon, and tend to obfuscate the underlying physics of the system. An alternative modeling approach that would reduce or eliminate the modeling artifacts was thus desired.

The artificial spikes could in principle be reduced to any desired level through mesh refinement. This approach was rejected for the FY14 SA because SDU simulations for slag oxidation and Tc release already require days of wall-clock time to complete, and additional grid resolution would make runtimes untenable. Instead the alternative concept of slag oxidation shown in Figure 3-1 (b) was developed for the FY14 SA. Here a sharp front separating fully oxidized and fully reduced subregions is assumed to be passing through the grid cell undergoing oxidation. Under this concept, Tc is released from the solid to the liquid phase uniformly over the period the oxidation front enters the cell until it leaves. The sorption coefficient transitions more gradually between the fully reduced to fully oxidized values (Figure 3-2(a)), leading to a more gradual release of Tc (Figure 3-2 (b)).

To derive a K_d function that implements this general concept, a simple advection-only (or advection-dominated) transport scenario is considered first, as depicted in Figure 3-3 (scenario ①). Here oxygen enters the cell through advection and Tc leaves the cell at the same Darcy velocity, U. The mass flowrate of Tc leaving the cell is

$$F = \frac{V}{\Delta z} c_L U \tag{2}$$

where V = total volume, Δz = cell height, and c_L = Tc liquid-phase concentration. Similarly, the mass flowrate of oxygen entering the cell is

$$G = \frac{V}{\Delta z} c_{Ox} U \tag{3}$$

where c_{Ox} = dissolved concentration of oxygen at solubility. An oxidation front moving through a cell effectively functions as a moving line source of Tc to the liquid phase. Oxidation at constant rate acts approximately as a constant source of Tc. Assuming that advection is sufficiently fast to sweep Tc from the cell and prevent an accumulation, then the mass rate of Tc leaving the cell should approximately match the constant source term. For a constant flow rate, this implies a constant liquid phase concentration, c_L. Under this assumption the depletion time for Tc is

$$\Delta t_F = \frac{m_{Tc,0}}{F} = \frac{m_{Tc,0}}{V c_L U/\Delta z} \tag{4}$$

Similarly, the concentration of dissolved oxygen is constant and the depletion time for slag reaction capacity is

$$\Delta t_G = \frac{m_{slag,0}}{G} = \frac{\rho_b V c_{slag,0}}{V c_{Ox} U/\Delta z} \tag{5}$$

Under these advective transport conditions, the speed of the oxidation front is $c_{Ox}U/c_{Slag,0}\rho_b$ compared to a pore velocity of U/Sn. For saltstone, S = 1 mL liquid / mL void, n = 0.58 mL void / mL, c_{Ox} = 1.06e-3 meq e-/mL liquid, $c_{slag,0}$ = 0.607 meq e-/g solid, ρ_b = 1.01 g solid/mL, and the rate of oxidation is three orders of magnitude slower than the rate of advective transport of a mobile species. Any Tc

released to the liquid will be advected out of the cell in short order compared to the rate of cell oxidation. Thus, Tc should be depleted at approximately the same time as slag reaction capacity. Equating Equations (4) and (5) and solving for c_L, after some algebra, produces

$$c_L = \frac{c_{T,0} c_{Ox}}{\rho_b c_{slag,0}} \tag{6}$$

The sorption coefficient is defined as

$$K_d \equiv \frac{c_s}{c_L} = \frac{m_s/\rho_b V}{c_L} = \frac{m - m_L}{\rho_b V c_L} = \frac{m - SnVc_L}{\rho_b V c_L} = \frac{m/V}{\rho_b c_L} - \frac{Sn}{\rho_b} = \frac{c_T}{\rho_b c_L} - \frac{Sn}{\rho_b} = \frac{c_{T,0}}{\rho_b c_L} \cdot \frac{c_T}{c_{T,0}} - \frac{Sn}{\rho_b} \tag{7}$$

The prior assumption that Tc and slag are depleted at the same rate implies

$$\frac{c_T}{c_{T,0}} = x_{Re} = (1 - x_{Ox}) = 1 - \frac{c_{slag}}{c_{slag,0}} \tag{8}$$

Equation (6) can also be rearranged as

$$\frac{c_{T,0}}{\rho_b c_L} = \frac{c_{slag,0}}{c_{Ox}} \tag{9}$$

Substituting Equations (8) and (9) into Equation (7) yields, the desired K_d functionality for redox conditions ($x_{Re} < 1$)

$$K_d{}^{redox} = \frac{c_{slag,0}}{c_{Ox}} x_{Re} - \frac{Sn}{\rho_b} \tag{10}$$

Note that this effective sorption coefficient is a function of only one time-varying quantity, $x_{Re} = 1 - x_{Ox}$. To avoid negative values of K_d and implement fully oxidized conditons ($x_{Re} = 0$), Equation (10) is modified to

$$K_d{}^{redox} = max\left[\frac{c_{slag,0}}{c_{Ox}} x_{Re} - \frac{Sn}{\rho_b}, K_{d,Ox}\right] \tag{11}$$

The K_d functionality needed to implement solubility control ($x_{Re} = 1$) is given by Jordan and Flach (2013, Equation 2.16) as

$$K_d{}^{solubility} = max\left[\frac{c_T - nSC_{sol}}{\rho_b C_{sol}}, K_{d,Re}\right] \tag{12}$$

The full range of conditions ($0 \le x_{Re} \le 1$) can be approximated by blending Equations (11) and (12) with an x_{Re} weighting function

$$K_d = {x_{Re}}^p K_d{}^{solubility} + (1 - {x_{Re}}^p) K_d{}^{redox} \tag{13}$$

A rapid transition from $K_d{}^{solubility}$ to $K_d{}^{redox}$ when a cell starts becoming oxidized requires $p \gg 1$. The somewhat arbitrary value $p = 200$ was deemed satisfactory in FY14 SA modeling.

Figure 3-4 compares application of Equation (13) to the FY13 SA Tc release sub-model for a single computational cell, with and without solubility control. Oxygen ingress, and thus cell oxidation, starts at

time zero and full oxidation occurs at t = 150 yrs. The top row of plots illustrate the spike release of Tc characteristic of the FY13 SA Tc release sub-model. In contrast, Equation (13) produces a nearly uniform Tc release consistent with a uniform oxidation rate. Figure 3-5 illustrates a similar simulation where oxygen ingress is delayed until t = 25 years, such that the first 25 years represents transport under fully reduced conditions. Solubility control is evident for the FY14 SA model (lower left plot). Figure 3-6 shows a stack of 10 cells containing slag and Tc, plus inlet and outlet cells. Figure 3-7 illustrates Tc flux results for the FY13 and FY14 SA models with and without solubility control. For the solubility control case, no Tc is released above the solubility limit until the final cell is no longer fully reduced. For the FY13 SA model, a very sharp flux spike occurs as the bottom cell approaches 100% oxidation. For the FY14 SA model the Tc release is approximately uniform over the period the cell is being oxidized. Figure 3-8 provides $K_{d,Re}$ = 10,000 mL/g results under no solubility control for comparison to 1000 mL/g results shown in Figure 3-7. In these advection-dominated transport simulations the FY14 SA model is observed to produce much smoother Tc flux results.

Figure 3-9 depicts the Discrete Fracture Model (DFM) considered previously by Jordan and Flach (2013, Figure 2-30). Here transport is advection-dominated within the fracture but diffusion-dominated in the surrounding matrix. Figure 3-10 compares the FY13 SA Tc release sub-model to Equation (13). The revised model is observed to produce significantly better results with and without solubility control. With no solubility control, flux spikes are nearly eliminated. However, with solubility control non-physical flux variability remains, although significantly dampened and more oscillatory compared to the FY13 SA results. The nature of oxygen and Tc transport for the DFM simulation is similar to scenario ② depicted in Figure 3-3. Oxygen enters the top through advection and the fracture side by diffusion. Tc leaves the bottom by advection and *both* sides by lateral diffusion. Assuming for the moment that the diffusion distance is one cell width, Δx, the Tc and oxygen mass flowrates equations analogous to Equations (2) and (3) are

$$F = \frac{V}{\Delta z} c_L U + 2 \frac{V}{\Delta x} D_e \frac{c_L}{\Delta x} \tag{14}$$

$$G = \frac{V}{\Delta z} c_{Ox} U + \frac{V}{\Delta x} D_e \frac{c_{Ox}}{\Delta x} \tag{15}$$

Note that Equation (14) contains a factor of two in the diffusion term, reflecting transport from both sides, whereas oxygen is available only from the fracture side. Following the same process as before, the result is

$$K_d{}^{redox} = f_{Pe} \frac{c_{slag,0}}{c_{Ox}} x_{Re} - \frac{Sn}{\rho_b} \tag{16}$$

where

$$f_{Pe} = 1 + \frac{1}{1 + Pe(\Delta x/\Delta z)^2} \tag{17}$$

and Pe is the Peclet number

$$Pe = \frac{U \Delta z}{D_e} \tag{18}$$

For advection-dominated transport, the Peclet number approaches infinity and $f_{Pe} \rightarrow 1$. Thus Equation (10) is recovered as a special case of Equation (16). For diffusion-dominated transport, Pe = 0 and f_{Pe} = 2, which effectively doubles the $K_d{}^{redox}$ value (the term Sn/ρ_b is small). Thus the range of f_{Pe} for

scenario ② in Figure 3-3 is $1 \leq f_{Pe} \leq 2$. Figure 3-11 shows the flux results for solubility control using Equation (16) and f_{Pe} values of 1.25, 1.5, 1.75, and 2. Increasing values of f_{Pe} are observed to improve the results by further reducing flux oscillations. Nonetheless, oscillations are still significant at f_{Pe}= 2.

Scenario ③ in Figure 3-3 likely explains the remaining discrepancy between model simulations and physical expectations. Once the oxidation front has penetrated the matrix, the diffusion distance for oxygen and Tc from and to the fracture, respectively, has lengthened considerably. However, the adjoining cell on the opposite side is reduced and maintains a low concentration sink for Tc at a short distance. Therefore, the diffusive ingress of oxygen is much slower than the diffusive egress of Tc for scenario ③ compared to scenario ②. This observation implies that an even larger value of f_{Pe} is needed for scenario ③. Figure 3-12 presents an empirical investigation of the optimal f_{Pe} value needed for the DFM case. Note that higher values of f_{Pe}indeed improve the flux results. An f_{Pe} value between 3 and 4 appears to be optimal. Simulation results for f_{Pe} = 3.5 are provided in Figure 3-13, in comparison to the FY13 SA approach, the FY14 SA advection-concept (f_{Pe} = 1), the FY14 SA diffusion-dominated case for Figure 3-3 scenario ② (f_{Pe} = 2), and the FY14 SA empirical optimization value ($f_{Pe} \approx 3.5$). The latter model provides a marked improvement over the FY13 SA baseline.

Other scenarios of increasing sophistication could be considered, resulting in additional K_d functions. One possibility would be to monitor evolving transport conditions on a cell-by-cell basis and compute K_d on the fly using functions selected from a palette. However, considering the myriad of different K_d variations that might result from different transport scenarios, a focus on saltstone system modeling is helpful toward narrowing the possibilities. Except for relatively early periods (several hundred to a few thousand years), cementitious materials and the facility cover system are significantly degraded in the FY14 SA Nominal Value (NV) case. The result tends to be advection-dominated flow. Therefore, Equation (10) was selected for the redox term in Equation (13) for FY14 SA. Figure 3-14 shows the Tc flux for the SDU 2 FY13 SA evaluation case modified to use the FY14 SA Tc release sub-model. Figure 3-15 directly compares the FY13 and FY14 SA Tc release sub-models for the SDU 2 evaluation case from the FY13 SA. The FY14 SA Tc flux is observed to be relatively smooth until just past year 30,000 when the downward moving oxidation front breaches the concrete floor. After 30,000 years, the response is noticeably less spikey than the FY13 SA results. Figure 3-16 compares the FY13 and FY14 SA Tc release sub-models for the 20% oxygen source sensitivity case. Again, the FY14 SA model produces significantly smoother flux results that are more consistent with physical expectations.

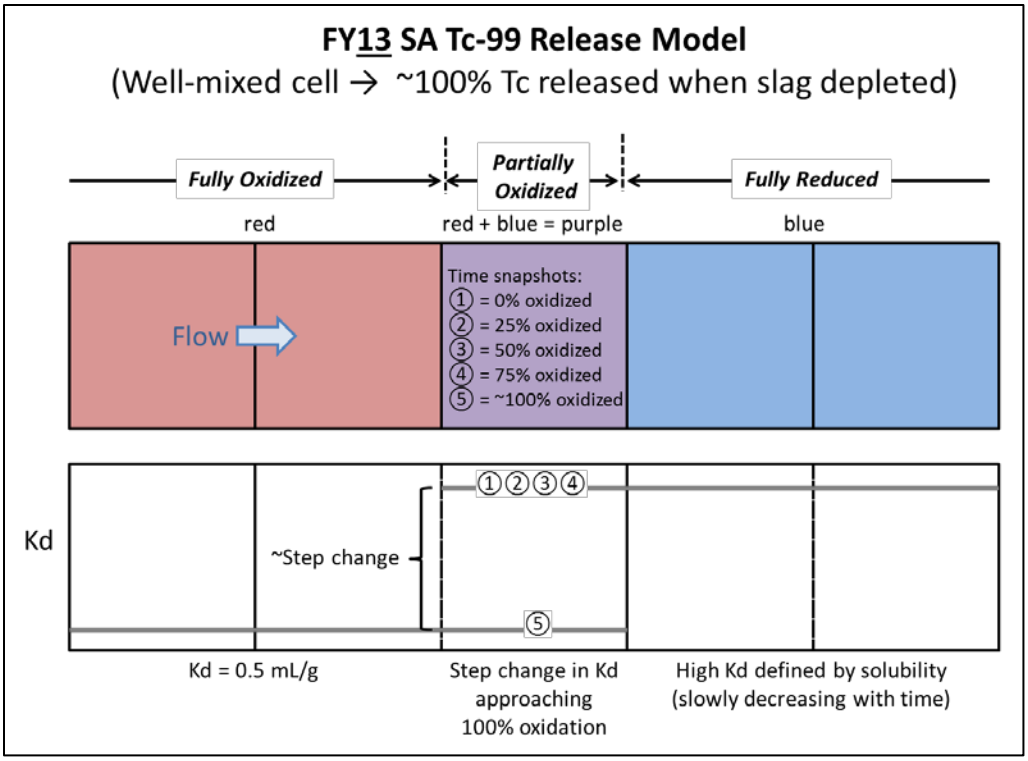

(a)

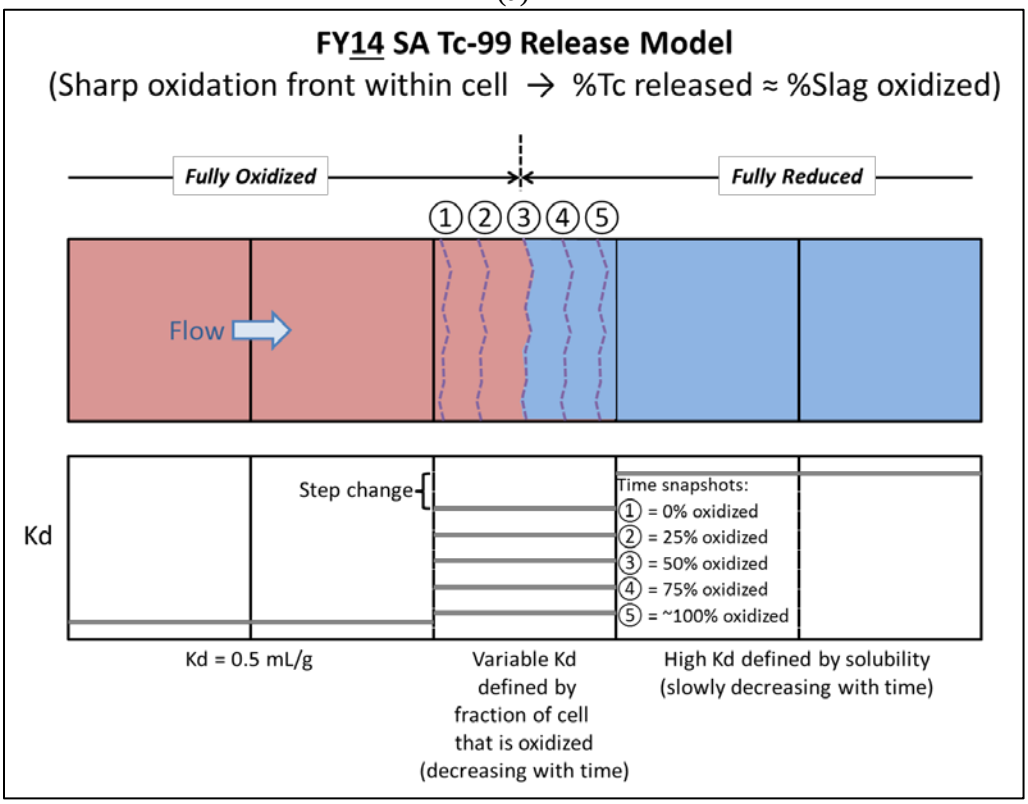

(b)

Figure 3-1. FY13 and FY14 SA concepts for Tc release within an oxidizing grid cell.

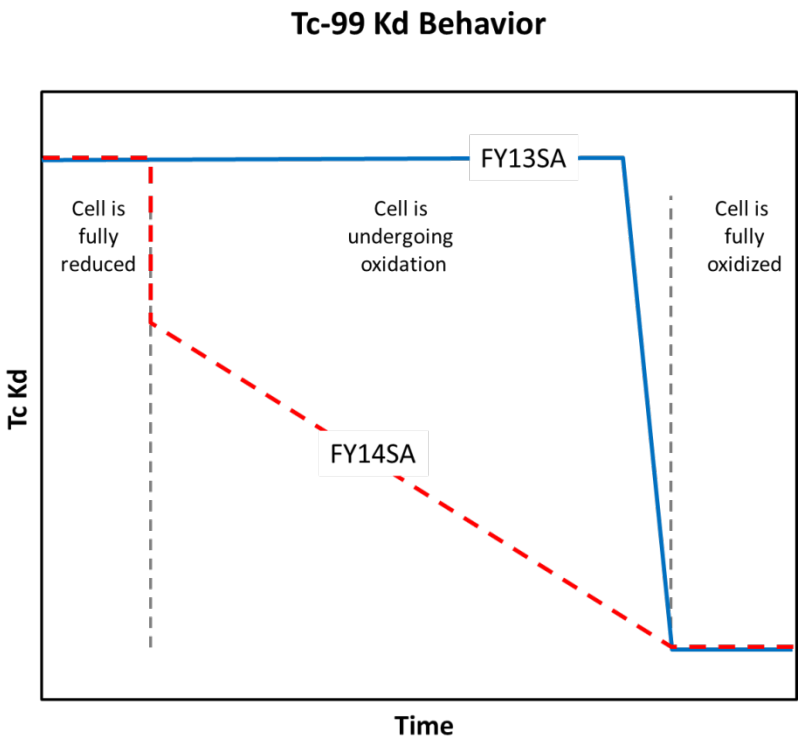

(a)

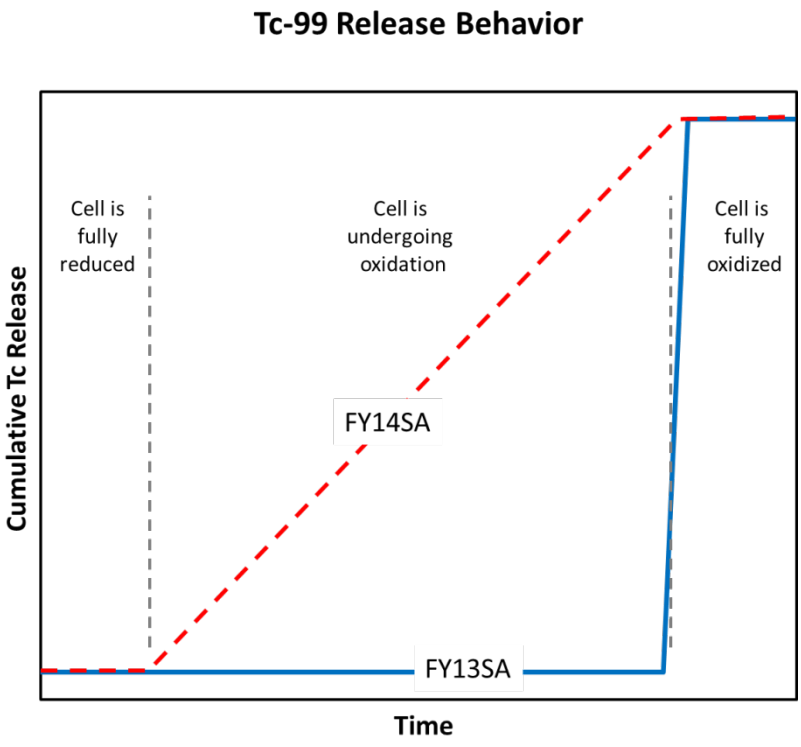

(b)

Figure 3-2. Comparisons of Tc-99 (a) sorption coefficient and (b) release behaviors for the FY13 and FY14 SA sub-models.

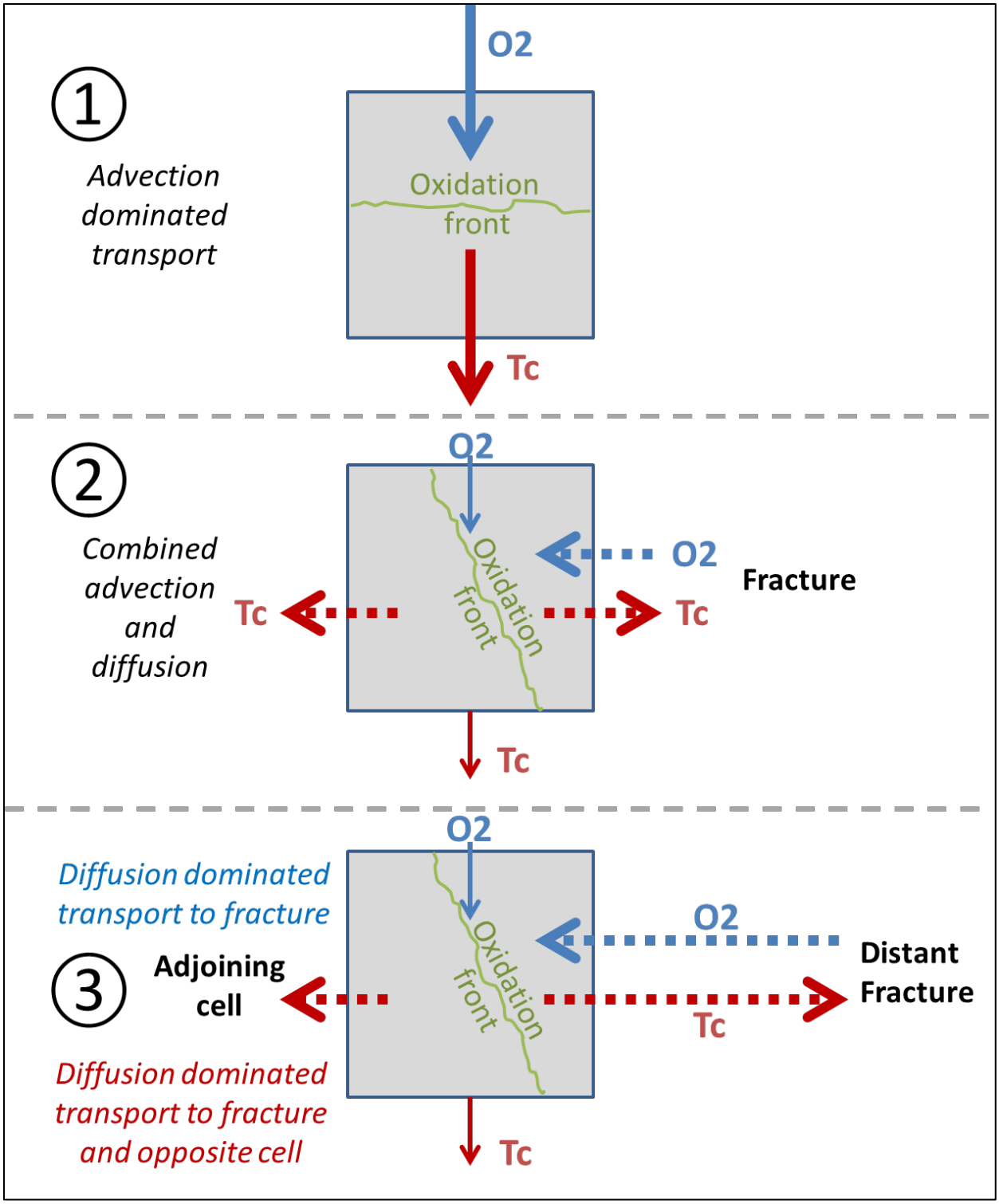

Figure 3-3. Oxidation and transport scenarios for oxygen and Tc.

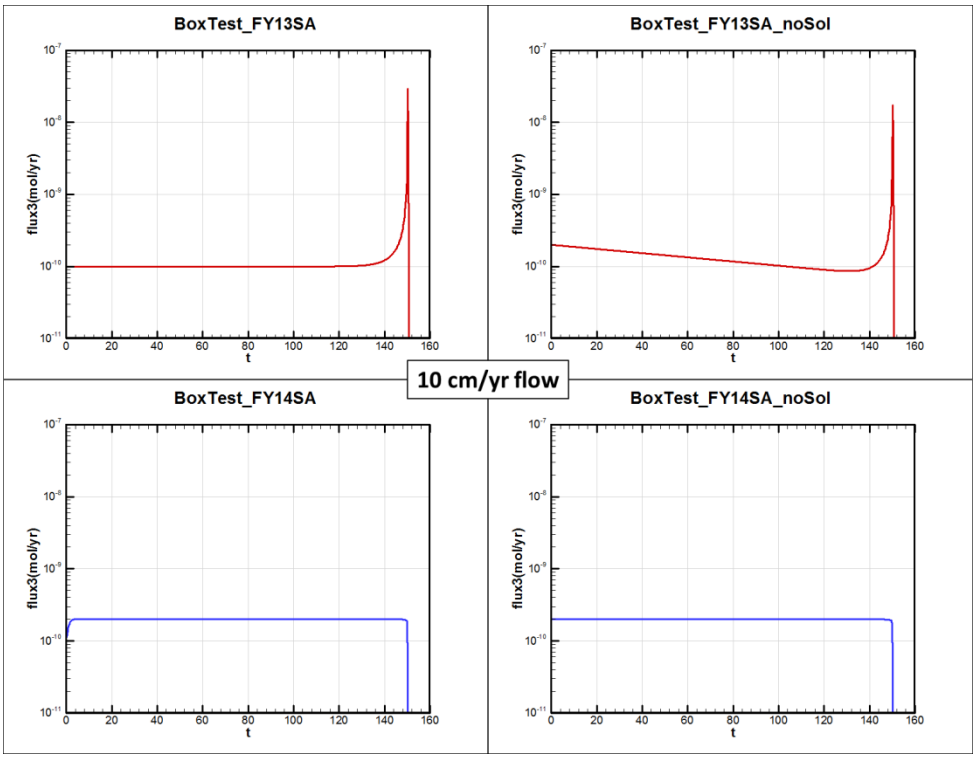

Figure 3-4. Slag oxidation and Tc transport simulation for a single grid cell with oxygen exposure from time zero ("BoxTest").

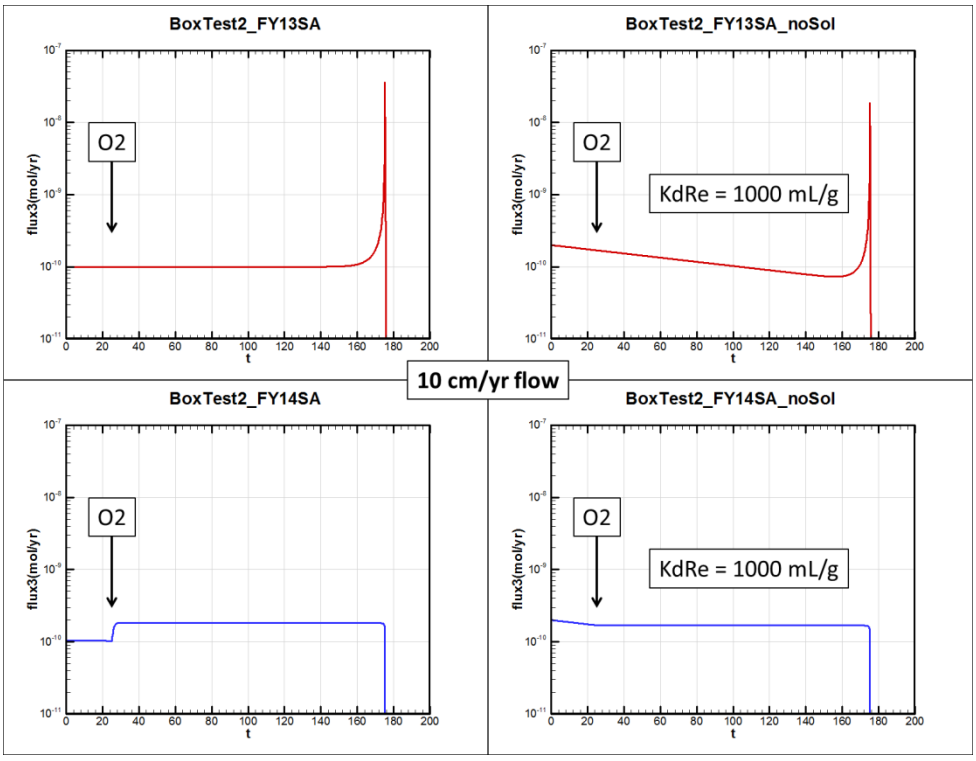

Figure 3-5. Slag oxidation and Tc transport simulation for a single grid cell with oxygen exposure starting at t=25 yr ("BoxTest2").

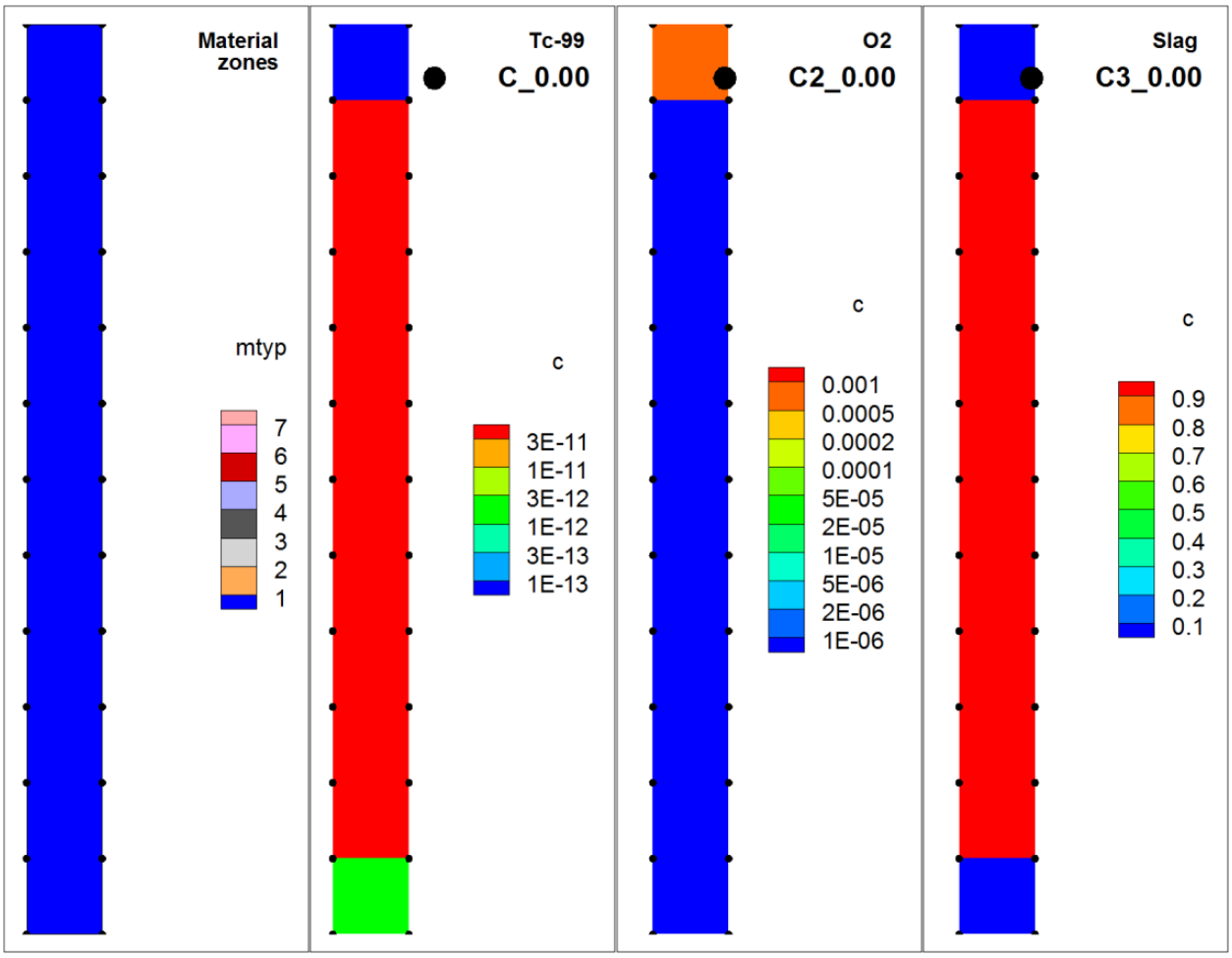

Figure 3-6. Stack of 10 slag and Tc bearing grid cells; condition at time zero.

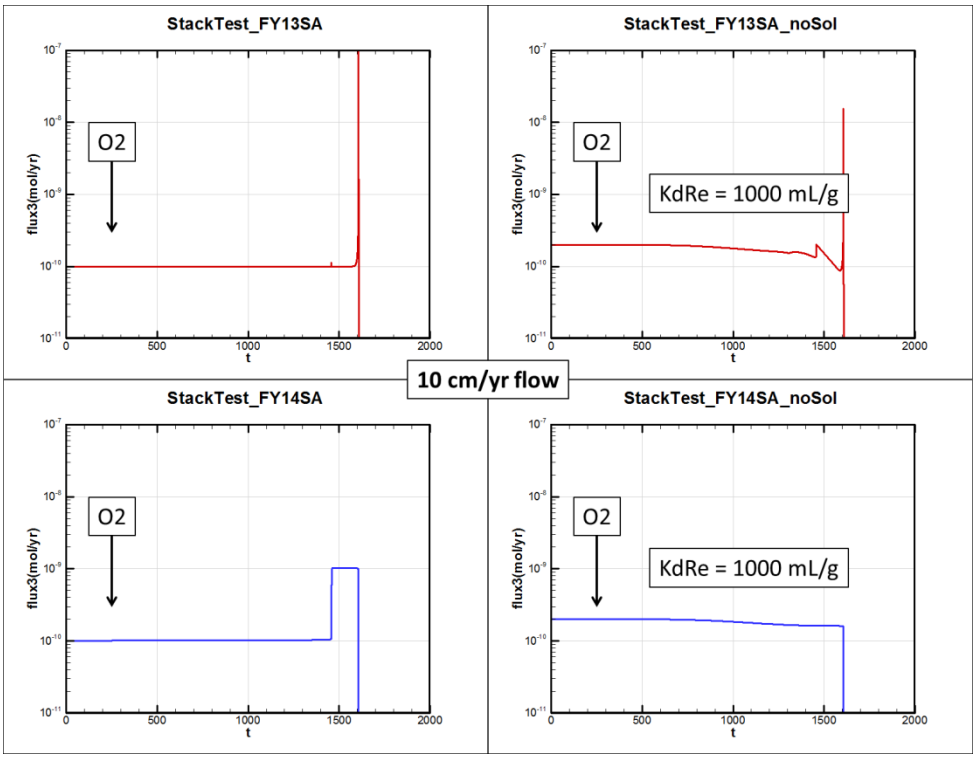

Figure 3-7. Slag oxidation and Tc transport simulation for a stack of cells with oxygen exposure starting at t=25 yr ("StackTest"); *Kd*Re = 1000 mL/g for no solubility cases.

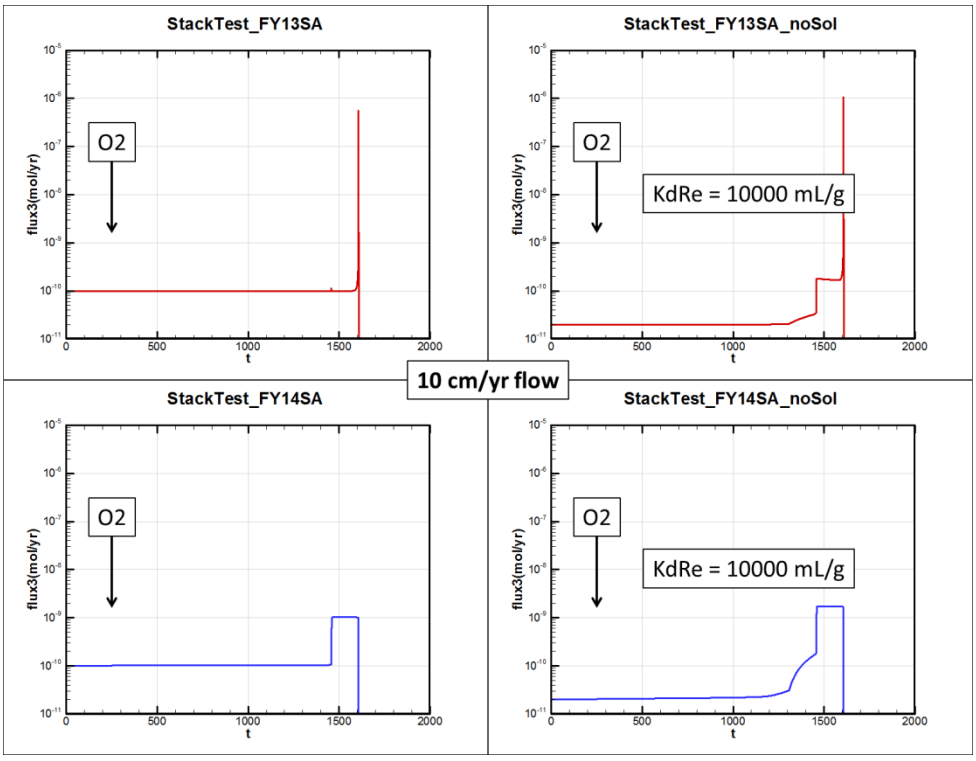

Figure 3-8. Slag oxidation and Tc transport simulation for a stack of cells with oxygen exposure starting at t=25 yr ("StackTest"); *Kd*Re = 10,000 mL/g for no solubility cases.

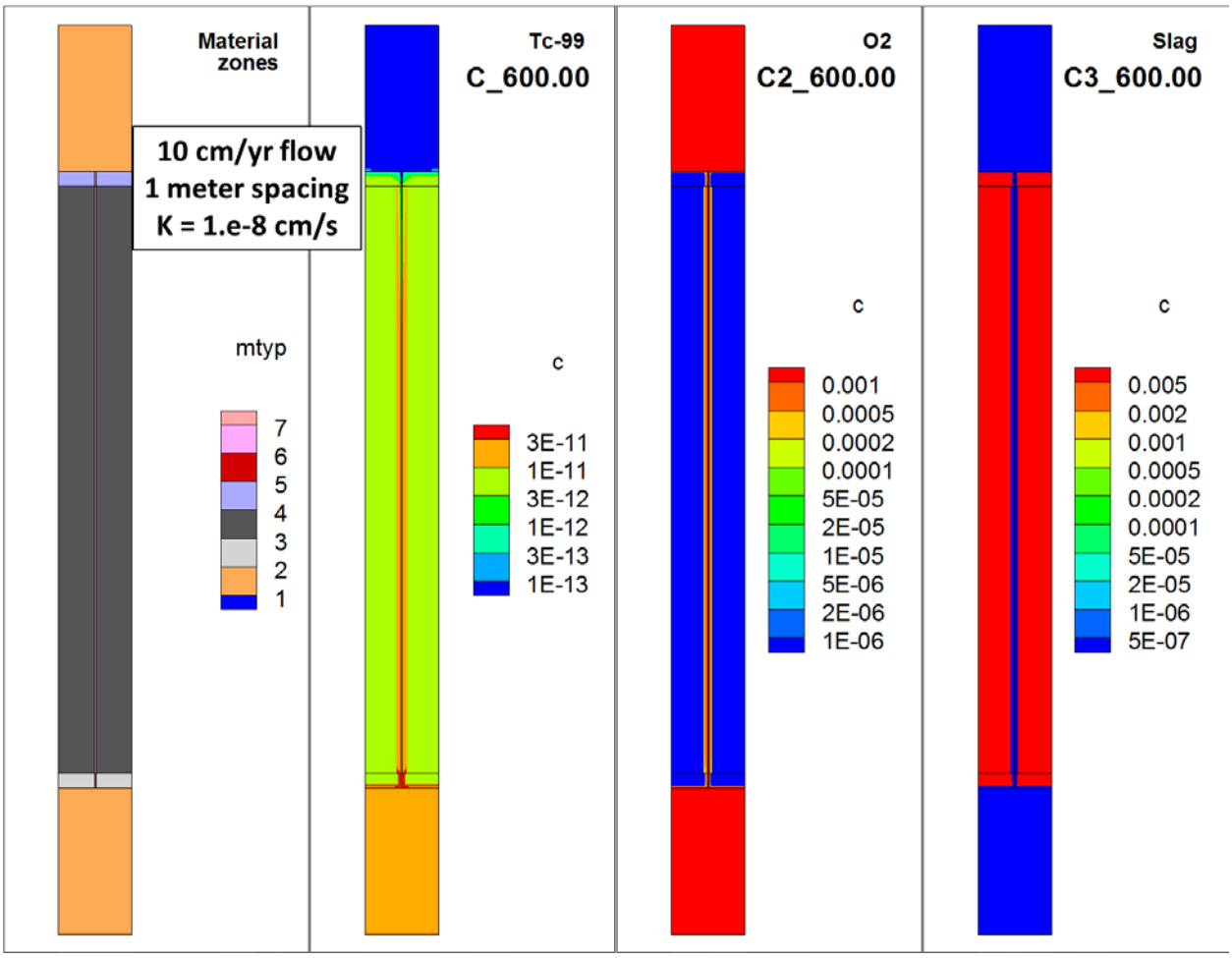

Figure 3-9. Discrete Fracture Model (DFM) simulation of slag oxidation and Tc transport; representative spatial snapshot at t=600 yrs.

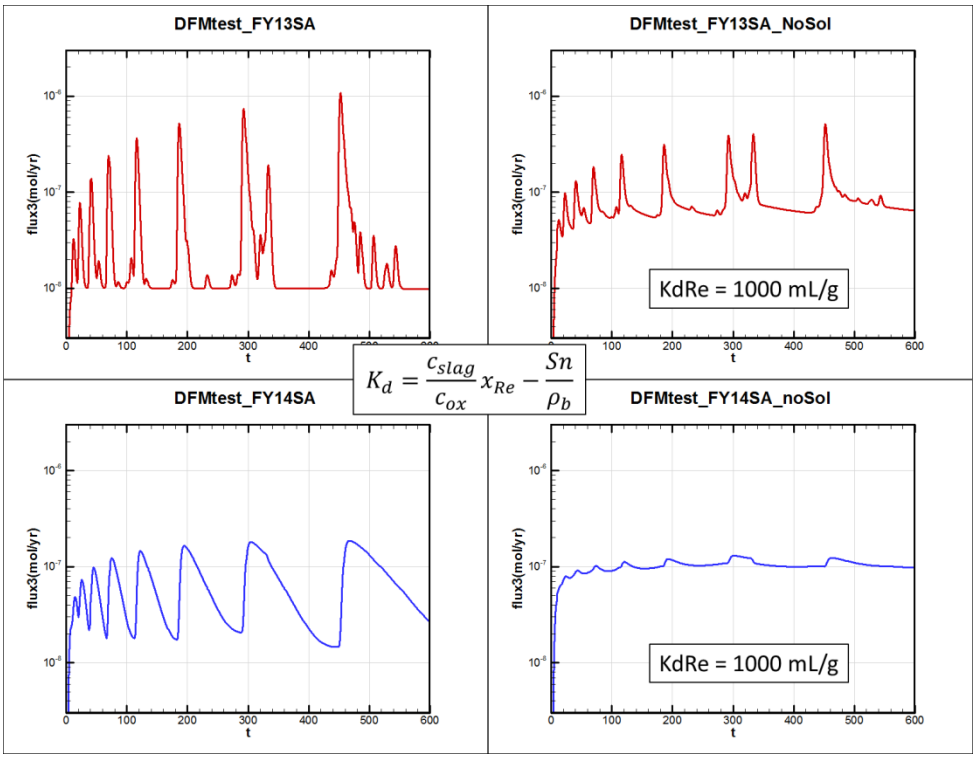

Figure 3-10. Comparison of DFM simulations for the FY13 to FY14 SA Tc release sub-models; FY14 SA sorption coefficient (*Kd*) based on advection-only concept.

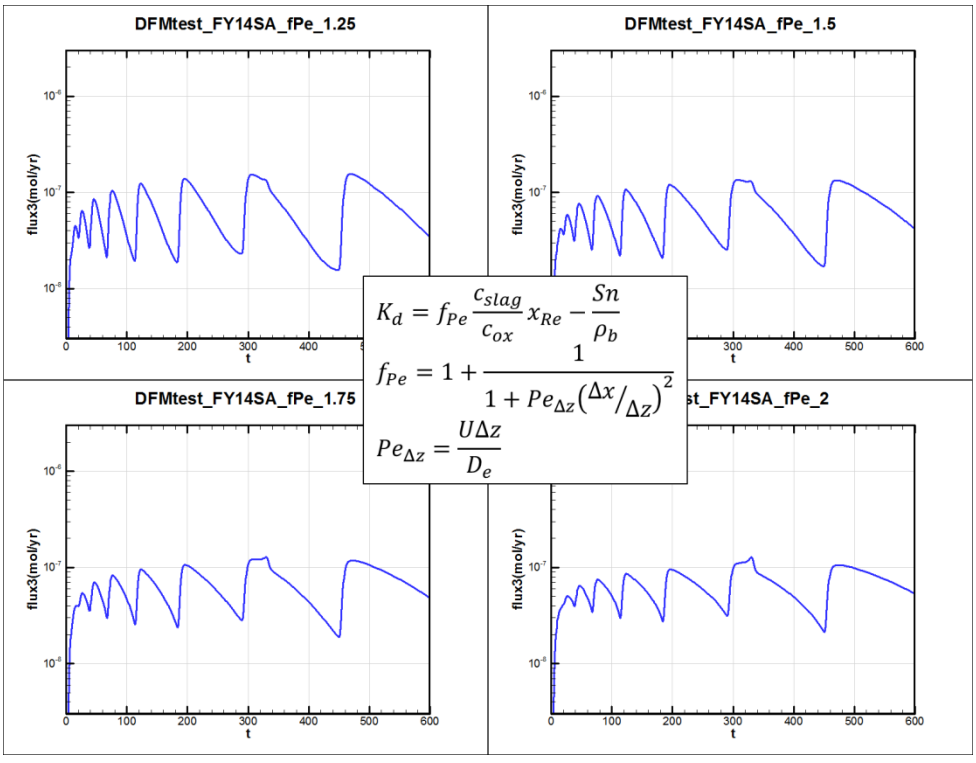

Figure 3-11. DFM simulations of slag oxidation and Tc transport using FY14 SA sorption coefficient (*Kd*) based on combined advection-diffusion concept ($1 < f_{Pe} \leq 2$).

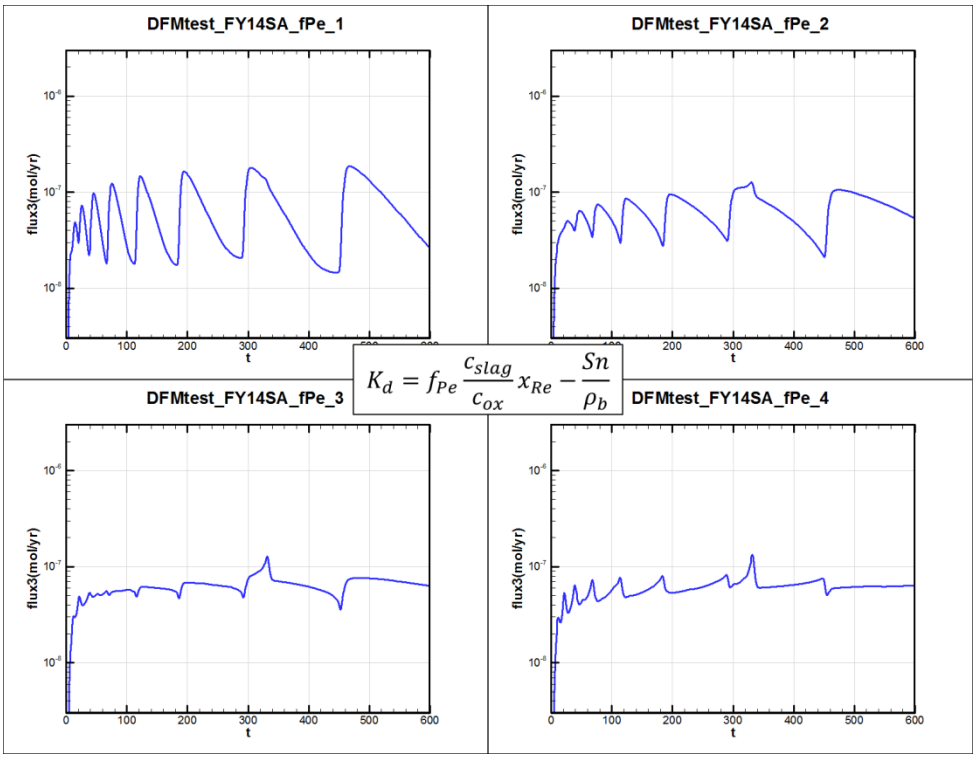

Figure 3-12. DFM simulations using FY14 SA Tc release sub-model with empirical coefficient values: f_{Pe} = 1, 2, 3, 4.

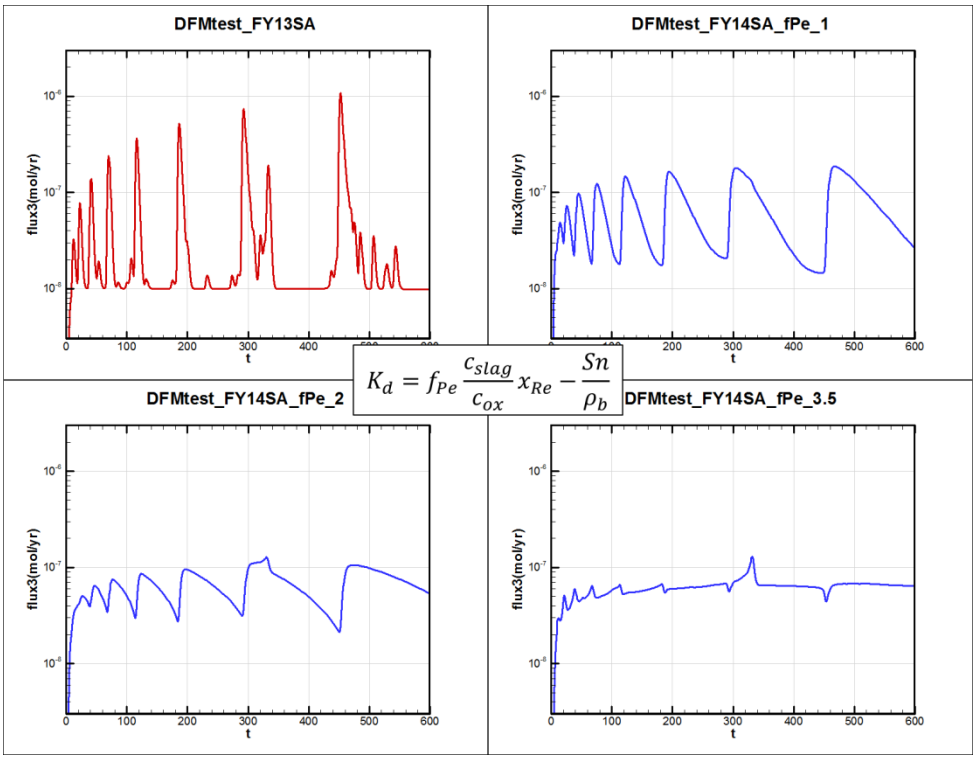

Figure 3-13. Summary of DFM simulation of slag oxidation and Tc transport.

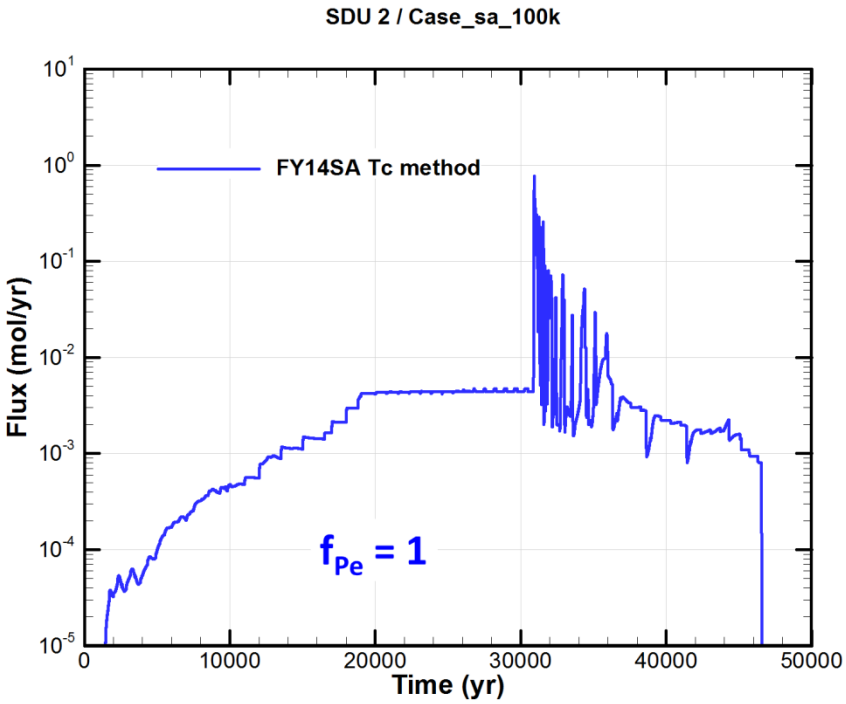

Figure 3-14. Slag oxidation and Tc transport simulation for SDU 2 evaluation case scenario using FY14 SA Tc release sub-model.

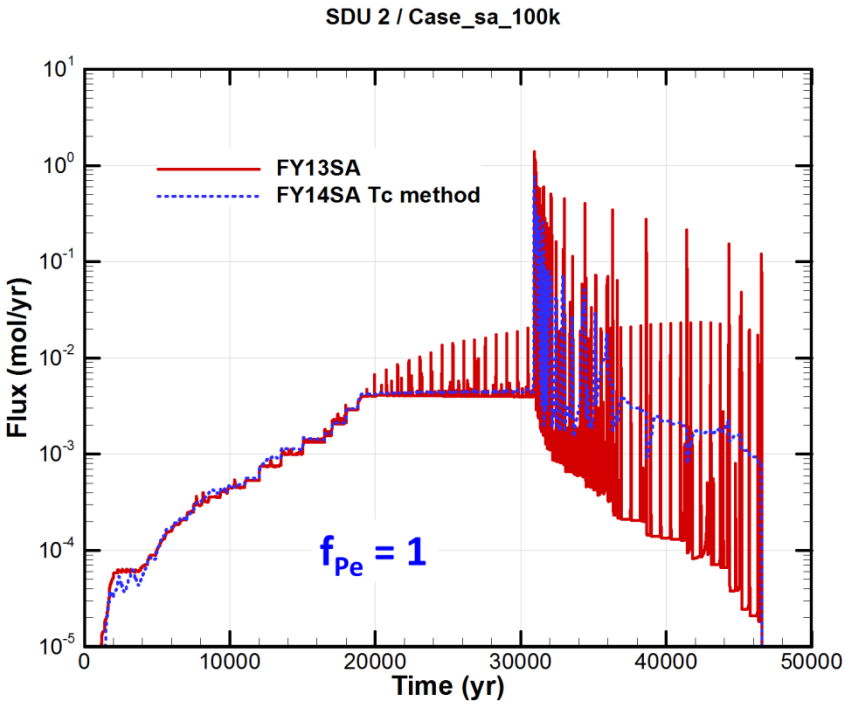

Figure 3-15. Comparison of FY13 and FY14 SA Tc release sub-models for SDU 2 evaluation case scenario.

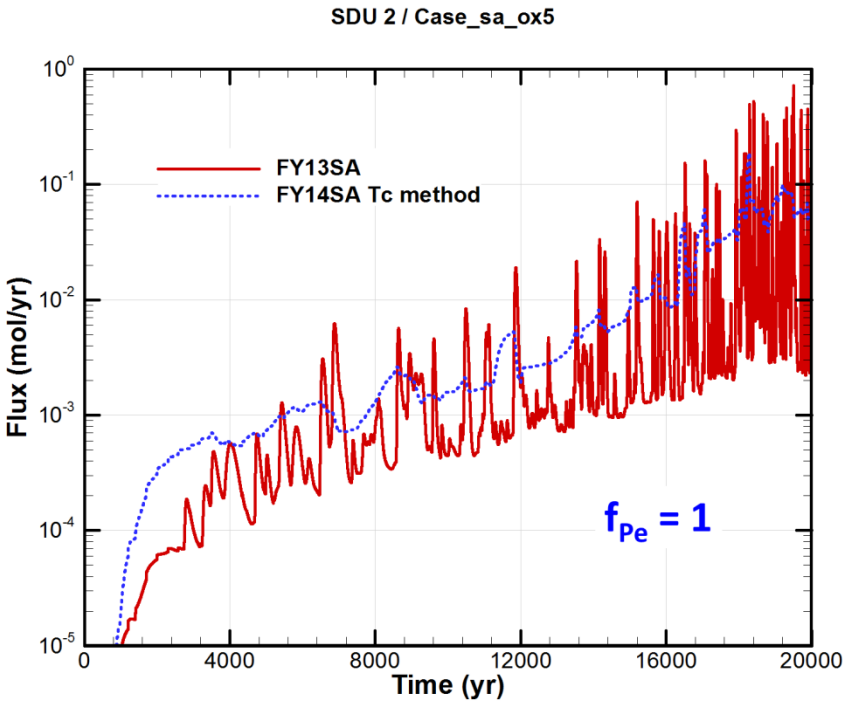

Figure 3-16. Comparison of FY13 and FY14 SA Tc release sub-models for SDU 2 20% oxidized cell sensitivity case.

4.0 Simulation Results

Representative FY14 SA simulation results are presented in this section, focusing on Tc-99 transport and a new dispersion sensitivity case. Figure 4-1 compares simulated Tc flux to the water table for the FY13 and FY14 Special Analyses. Note that several inventory estimates have been modified. The FY14 SA flux curves are significantly smoother than those for the FY13 SA as a result of implementing the revised Tc release sub-model in the FY14 SA. Figure 4-2 illustrates sensitivity results for internal oxygen sources in the proportions of 5, 10 and 20% compared to the evaluation case. Comparable simulations were performed in the FY13 SA (not shown), and the FY14 SA flux simulations are again markedly smoother.

Figure 4-3 shows the effect of dispersion added to the SALTSTONE region, which may be physically heterogeneous due to multiple pours/lifts resulting in cold joints, and partial phase separation (settling of suspended solids) within each lift. To assess sensitivity to dispersion assumptions, the longitudinal dispersity was set 1 meter (very roughly 10% of zone height, following the modeling practitioner's rule of thumb for aquifer transport) and the transverse dispersivity to 0.1 meter. The other material zones are assumed to be homogeneous and retain zero dispersivities as in Case_sa. As expected for I-129, the leading and trailing tails are higher and the peak concentration lower than the reference case. For Tc-99, the addition of dispersion has little impact on flux while the release is solubility-controlled. Later, when the oxidation front approaches and breaks through the floor, added dispersion produces a somewhat smoother, more sustained, release.

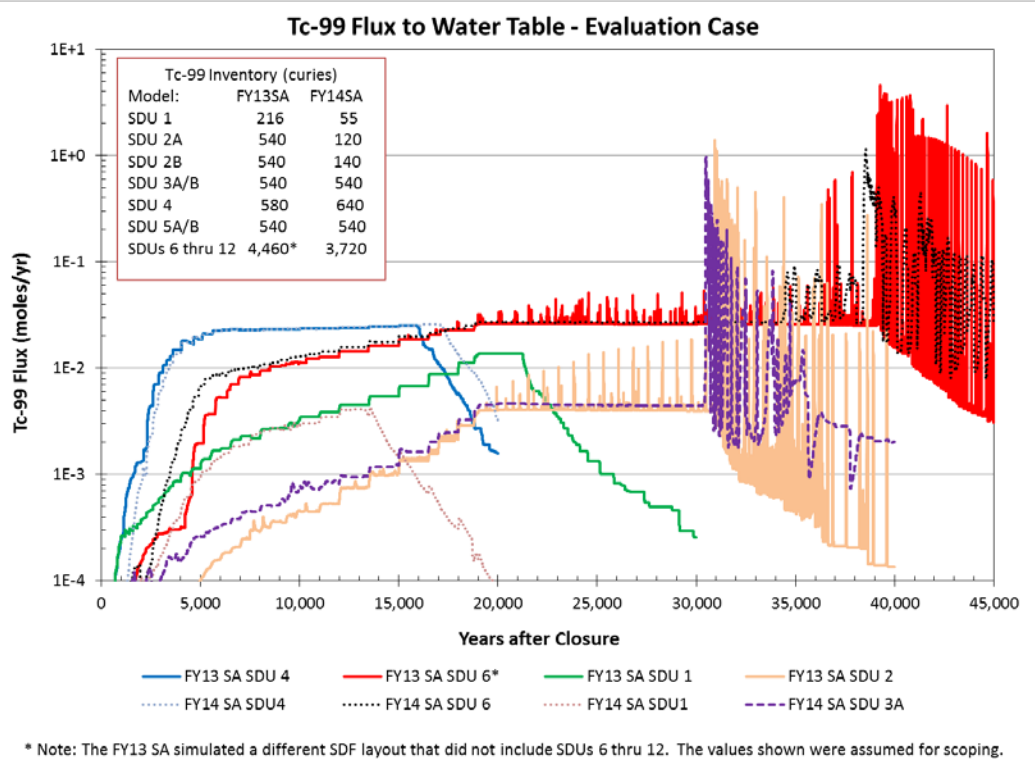

Figure 4-1. Comparison of FY13 and FY14 SA evaluation case Tc transport results for SDU design types 1, 2, 4 and 6.

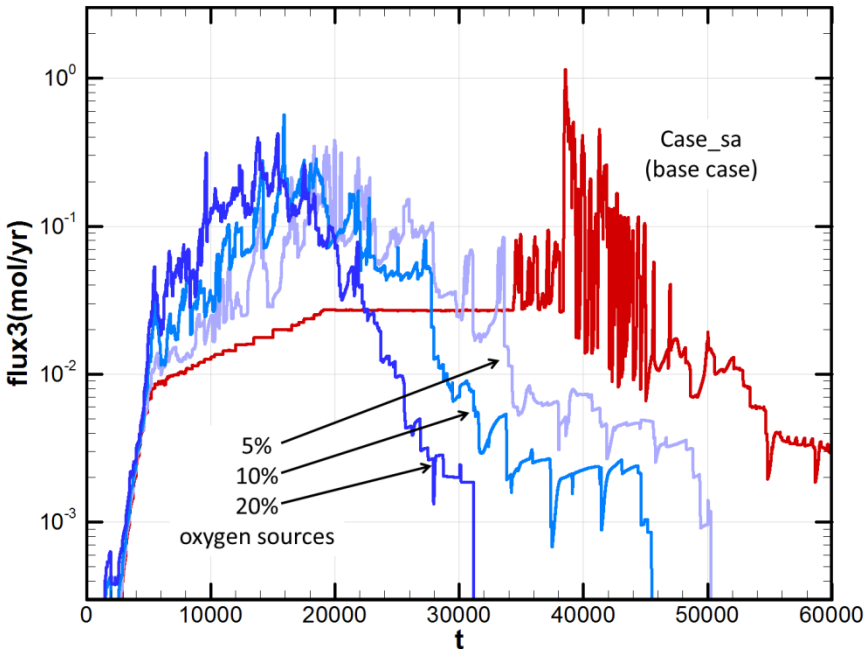

Figure 4-2. FY14 oxygen source sensitivity simulations compared to the SDU 6 evaluation case.

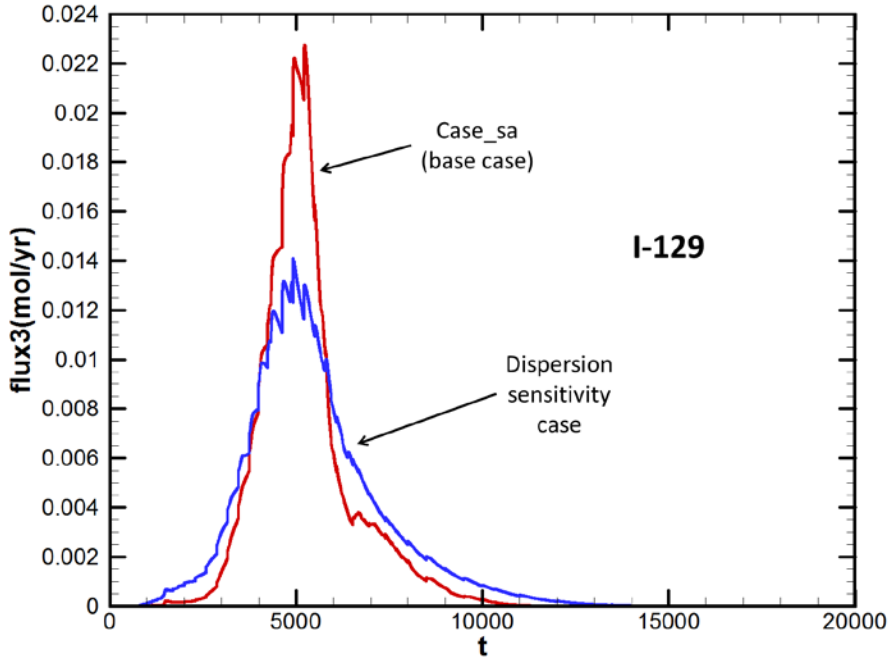

(a)

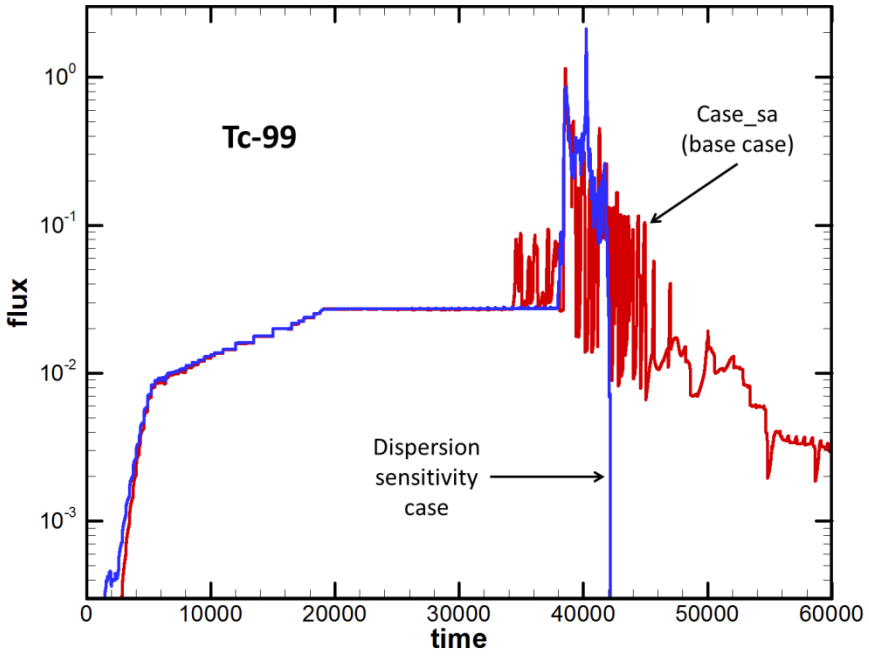

(b)

Figure 4-3. FY14 dispersion sensitivity simulations compared to the SDU 6 evaluation case: (a) I-129, (b) Tc-99.

5.0 References

Flach, G., *Completion of PORFLOW Modeling Supporting the Saltstone No Clean Cap UWMQE,* SRNL-L3200-2013-00048, December 4, 2013.

Flach, G. P. and F. G. Smith III, *Degradation of Cementitious Materials Associated with Saltstone Disposal Units*, SRNL-STI-2013-00118, Rev. 1, November 2013.

Jordan, J. M. and G. P. Flach, *PORFLOW Modeling Supporting the FY13 Saltstone Special Analysis*, SRNL-STI-2013-00280, Rev. 0, May 2013.

Kaplan, D. I. and T. Hang, *Estimated duration of the subsurface reducing environment produced by the Z-Area Saltstone Disposal Facility (U)*, WSRC-RP-2003-00362, Rev. 2. January 2003.

Kaplan, D. I. and D. Li, *Solubility of Technetium Dioxides (TcO_2-c, $TcO_2 \cdot 1.6H_2O$ and $TcO_2 \cdot 2H_2O$) in Reducing Cementitious Material Leachates: A Thermodynamic Calculation*, SRNL-STI-2012-00769, Rev. 1, February 2013.

Sheppard, R. E., *30 Million Gallon Saltstone Disposal Unit (SDU) PORFLOW Modeling for SDU-6 Special Analysis (SA)*, HLW-SSF-TTR-2013-0021, Rev. 2, October 23, 2013.

SRR Closure & Waste Disposal Authority, *FY2013 Special Analysis for the Saltstone Disposal Facility at the Savannah River Site*, SRR-CWDA-2013-00062, Rev. 0, June 2013.

SRR Closure & Waste Disposal Authority, *FY2014 Special Analysis for the Saltstone Disposal Facility at the Savannah River Site*, SRR-CWDA-2014-00006, Rev. 0, March 2014 draft.

Taylor, G. A., *Task Technical and Quality Assurance Plan for 30 Million Gallon Saltstone Disposal Unit (SDU) PORFLOW Modeling for SDU-6 Special Analysis (SA)*, SRNL-RP-2013-00396, October 2013.

This page intentionally left blank

Distribution:

R. S. Aylward, 773-42A
S. L. Marra, 773-A
E. N. Hoffman, 999-W
K. H. Rosenberger, 705-1C
M. Layton, 705-1C
S. P. Simner, 705-1C
P. R. Jackson, DOE-SR, 703-46A
B. T. Butcher, 773-43A
D. A. Crowley, 773-43A
G. P. Flach, 773-42A
F. G. Smith, III 703-41A
G. A. Taylor, 773-43A
Records Administration (EDWS)